Editors' Suggestion

Isotropic Quantum Griffiths Singularity in $Nd_{0.8}Sr_{0.2}NiO_2$ Infinite-Layer Superconducting Thin Films

Qiang Zhao,[1,*] Ting-Na Shao,[1,2,*] Wen-Long Yang,[1] Xue-Yan Wang,[1] Xing-Yu Chen,[1] Mei-Hui Chen,[1] Fang-Hui Zhu,[1] Cheng-Xue Chen,[1] Rui-Fen Dou,[1] Chang-Min Xiong,[1] Haiwen Liu,[1,3,4,†] and Jia-Cai Nie[1,3,‡]

[1]*School of Physics and Astronomy, Beijing Normal University, Beijing 100875, People's Republic of China*
[2]*Institute of System Engineering, AMS, PLA, Beijing 100020, People's Republic of China*
[3]*Key Laboratory of Multiscale Spin Physics, Ministry of Education, Beijing Normal University, Beijing 100875, People's Republic of China*
[4]*Interdisciplinary Center for Theoretical Physics and Information Sciences, Fudan University, Shanghai 200433, People's Republic of China*

(Received 17 December 2023; revised 7 April 2024; accepted 28 May 2024; published 17 July 2024)

This work reports on the emergence of quantum Griffiths singularity (QGS) associated with the magnetic field induced superconductor-metal transition (SMT) in unconventional $Nd_{0.8}Sr_{0.2}NiO_2$ infinite layer superconducting thin films. The system manifests isotropic SMT features under both in-plane and perpendicular magnetic fields. Importantly, after scaling analysis of the isothermal magnetoresistance curves, the obtained effective dynamic critical exponents demonstrate divergent behavior when approaching the zero-temperature critical point B_c^*, identifying the QGS characteristics. Moreover, the quantum fluctuation associated with the QGS can quantitatively explain the upturn of the upper critical field around zero temperature for both the in-plane and perpendicular magnetic fields in the phase boundary of SMT. These properties indicate that the QGS in the $Nd_{0.8}Sr_{0.2}NiO_2$ superconducting thin film is isotropic. Moreover, a higher magnetic field gives rise to a metallic state with the resistance-temperature relation $R(T)$ exhibiting $\ln T$ dependence among the 2–10 K range and T^2 dependence of resistance below 1.5 K, which is significant evidence of Kondo scattering. The interplay between isotropic QGS and Kondo scattering in the unconventional $Nd_{0.8}Sr_{0.2}NiO_2$ superconductor can illustrate the important role of rare region in QGS and help to uncover the exotic superconductivity mechanism in this system.

DOI: 10.1103/PhysRevLett.133.036003

The unconventional superconductivity in infinite-layer nickelates [1] resembles cuprate superconductors and have generated great research interest recently [2–17]. Although theoretical research predicts antiferromagnetic correlations in the NiO_2 plane [5,18–22], unlike cuprate superconductivity, the ground states in the parent $NdNiO_2$ and $LaNiO_2$ do not exhibit antiferromagnetic long-range order and show metallic behavior [23,24]. Features of short-range magnetic order or spin glass are found in various experimental works [25–28]. These differences between nickelate and cuprate superconductivity may be ascribed to the combination of self-doped Mott physics and the Kondo effect in nickelates [4,11,14,29–31], which requires further experimental evidence to confirm.

The pronounced inhomogeneities, such as impurities and defects originating from the *ex situ* growth of nickelate superconducting samples [1,32–36], may also disrupt the long-range antiferromagnetic order. Moreover, scanning transmission electron microscopy experiments also report the vertical structural defects of the Ruddlesden-Popper type formed on top of the sample surface [35,37,38]. Such quenched disorder effects can dramatically change the universality of critical behavior of superconductor-metal transition (SMT) and give rise to quantum Griffiths singularity (QGS) [39–47], as a generalization of classical Griffiths singularity [48]. However, the magnetic field induced QGS is mainly present in conventional superconductors [40–45,49,50]; whether this exotic quantum critical phenomenon can exist in unconventional superconductors is still unexplored.

Here, we report the observation of the isotropic QGS associated with SMT under both in-plane and perpendicular magnetic fields in unconventional $Nd_{0.8}Sr_{0.2}NiO_2$ superconducting thin film. The QGS characteristics are verified by finite-size scaling analysis of magnetoresistance under these two cases, and the obtained zero-temperature critical magnetic fields (B_c^*) of QGS exhibit isotropic features, largely different from QGS behaviors in conventional superconductors [49,50]. Moreover, the QGS fluctuation can provide quantitative explanations for the pronounced upturn of upper critical field (H_{c2}) in the phase boundary of SMT, which shares similar features with previously reported H_{c2} [51–54]. Such isotropic QGS features may originate from the competition of superconducting

fluctuation and Kondo scattering in $Nd_{0.8}Sr_{0.2}NiO_2$ superconducting thin films and generate further investigation on QGS in unconventional superconductors.

The infinite-layer $Nd_{0.8}Sr_{0.2}NiO_2$ thin films were fabricated by pulsed-laser deposition of the perovskite $Nd_{0.8}Sr_{0.2}NiO_3$ on $(001)SrTiO_3$ substrates, followed by soft-chemistry reduction [55]. Standard four probe method was utilized to perform the transport measurements. The high magnetic field (0–36 T) measurements were carried out by Hefei Steady-State High Magnetic Field Facilities in High Magnetic Field Laboratory, Chinese Academy of Sciences and University of Science and Technology of China [55]. As shown in Fig. 1(a), we have used the Aslamazov-Larkin (AL) formula to determine the superconducting transition temperature T_c^{AL} [70]. The obtained T_c^{AL} of a typical 7.6-nm-thick $Nd_{0.8}Sr_{0.2}NiO_2$ superconducting film is about 7.72 K and close to the temperature corresponding to $0.5R_n$. T_c^{zero}, about 3.00 K, is identified as the temperature at which the R_s drops beyond the measurement limit. The measured I-V characteristics at different temperatures are shown in Fig. 1(b), where the critical current density J_C (voltage criterion ~0.1 V/cm) approaches 9.63×10^4 A cm^{-2} at $T = 2$ K. With increasing magnetic field to large value, the superconductivity is suppressed. The isomagnetic $R_s(T)$ shows that sheet resistance changes very slightly at the ultralow temperatures with a zero-temperature critical field (around 19 T),

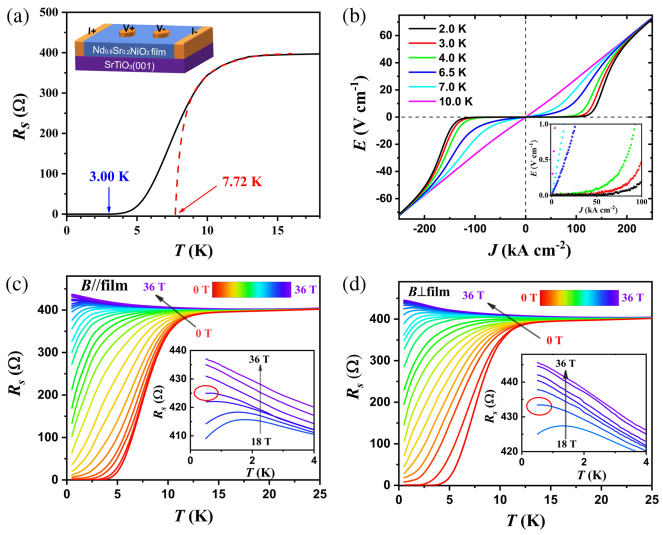

FIG. 1. Magnetic field induced SMT. (a) Temperature dependence of sheet resistance $R_s(T)$ under zero magnetic field. The dashed red line is the fits to 2D AL formula for a representative resistive transition. (b) Electric field (E) versus current density (J) characteristics for varying temperature. The enlarged image is shown in the inset to achieve high accuracy. Isomagnetic $R_s(T)$ curves under in-plane (c) and perpendicular (d) magnetic fields. The insets are the enlarged views in low-temperature regime with a magnetic field range of 18–36 T. The red circles indicate the R_s platforms of 19.5 T and 19.0 T at the lowest temperatures, under the in-plane and perpendicular magnetic field, respectively.

as shown in Figs. 1(c) and 1(d). We can see more clearly from the insets of Figs. 1(c) and 1(d) that a resistance plateau (indicated by the red circles) appears when the in-plane magnetic field ($B_{//}$) is about 19.5 T and the perpendicular magnetic field ($B_\perp$) is about 19.0 T. The isotropic features of the critical field are largely different from those anisotropic features in conventional two-dimensional superconductors [44,71–73]. As the magnetic field increases further, the sheet resistance continues to increase with the decrease of temperature at extremely low temperatures, namely a weakly localized metal behavior [42,49,50,74]. Thus, the thin film undergoes a quantum phase transition from a superconducting state to a metal with a critical resistance (426.0 Ω for in-plane, 432.7 Ω for perpendicular magnetic field) much smaller than the quantum resistance $h/4e^2 \approx 6.45$ kΩ (here h is the Planck constant and e is the elementary charge), as shown in the insets of Figs. 1(c) and 1(d).

The magnetoresistance $R_s(B)$ curves measured at different temperatures cross each other, as shown in Fig. S2 of the Supplemental Material. However, as shown in Figs. 2(a) and 2(b) for the low temperature regime (< 3 K), $R_s(B)$ curves intersect with each other to form a cross line in a transition region rather than a critical point. Figures 2(c) and 2(d) show the intersection points of the two adjacent temperature curves of isothermal magnetoresistance

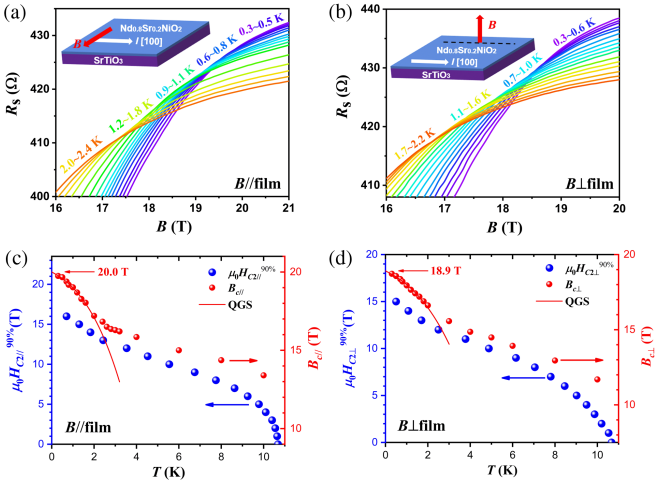

FIG. 2. (a) $R_s(B)$ curves at various temperatures ranging from 0.3 to 2.4 K under in-plane magnetic field. The inset is the experimental configuration. The direction of the magnetic field is applied along [010], perpendicular to the direction of the current applied along [100]. (b) $R_s(B)$ curves measured under perpendicular magnetic field at various temperatures from 0.3 to 2.2 K. The red circles in (c) and (d) show the cross points of the isothermal magnetoresistance curves at every two adjacent temperatures under in-plane and perpendicular magnetic field, respectively. And the red solid lines are the fitting curves based on the activated scaling analysis, and the fitting parameters are given in Table S-III. [55]. The blue circles in (c) and (d) show the temperature dependence of $H_{c2}^{90\%}$, denoting the field strength at which the resistivity reaches 90% of the normal state.

obtained under in-plane and perpendicular magnetic field, respectively [data extracted from Figs. 2(a) and 2(b)]. The continuous crossing points, shown as the red circles in the Figs. 2(c) and 2(d), are completely different from the conventional SMT and exhibit a QGS behavior.

Remarkably, the anomalous upturns of $H_{c2,\perp}(T)$ and $H_{c2,//}(T)$ below 2 K are obviously beyond the conventional Werthamer-Helfand-Hohenberg and Klemm-Luther-Beasely theories [75,76]. Based on the activated scaling analysis of QGS [77], for both in-plane $B_{c//}-T$ and perpendicular $B_{c\perp}-T$ curves as shown by the solid red lines in Figs. 2(c) and 2(d), we use the relation $(B_c^*-B_c(T))/B_c^* \propto u[\ln(T^*/T)]^{-1/\nu\psi-y}$ (1) to fit the phase boundary $B_c(T)$ [49]. Here T^* is the temperature of quantum critical fluctuation, u is the leading irrelevant scaling variable, and $y > 0$ is the associate irrelevant exponent.

Figures 2(c) and 2(d) also demonstrate the low temperature dependences of $H_{c2,\perp}^{90\%}$ and $H_{c2,//}^{90\%}$, which correspond to the field strength at which the resistivity reaches 90% of the normal state under in-plane and perpendicular magnetic field, respectively. The $H_{c2}^{90\%}(T)$ and $H_{c2}^{50\%}(T)$ can also be well fitted by the activated scaling analysis [55]. The quantitative fit to both the phase boundaries $H_{c2,\perp}(T)$ and $H_{c2,//}(T)$ by the activated scaling analysis indicates the presence of QGS at extremely low temperatures.

In order to gain more information on the QGS, we utilize the finite-size scaling analysis to obtain the effective critical exponents, and the resistance takes the scaling form [40,42,49,50]: $R_s(B,T) = R_c f[|B-B_c|T^{-1/z\nu}]$ (2). Here, z is the effective dynamical critical exponent, and ν is the correlation length exponent, $f[]$ is an arbitrary function of B and T with $f[0] = 1$, and (R_c, B_c) denotes the crossing point of magnetoresistance curves $R_s(B)$ at given temperature region. For both the in-plane and perpendicular magnetoresistance curves, five representative crossing points with the corresponding $R_s(B)$ curves are shown in Fig. S7 in the Supplemental Material [55], and the finite-size scaling analysis gives the effective critical exponent $z\nu$. The error bars representing the width of the $z\nu$ value in Figs. 3(a) and 3(b) are acquired by considering both measurement and instrumental errors [78] during the scaling analysis [55]. The effective critical exponent $z\nu > 1$ follows the activated scaling law [79]: $z\nu \propto |B-B_c^*|^{-0.6}$ (3), when approaching characteristic field B_c^* and zero temperature [Figs. 3(a) and 3(b)]. Surprisingly, the characteristic magnetic fields $B_{c//}^*$ and $B_{c\perp}^*$ in Figs. 3(a) and 3(b) are very close. This isotropic QGS features are distinguished from the anisotropic QGS in previous experimental works, with the ratio of in-plane/perpendicular critical field $B_{c//}^*/B_{c\perp}^* \approx 4.9$ [49] and $B_{c//}^*/B_{c\perp}^* \approx 15.4$ [50]. Such isotropic QGS indicates that a certain microscopic mechanism beyond the vortex physics may dominate the critical behavior in the magnetic field driven SMT of $Nd_{0.8}Sr_{0.2}NiO_2$ thin films.

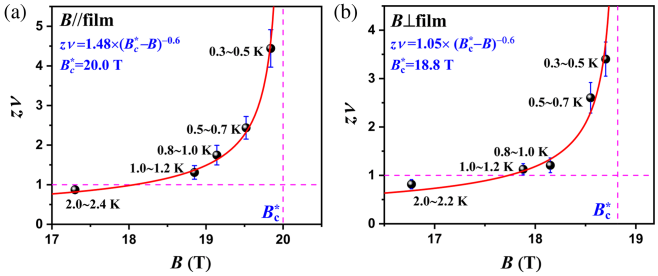

FIG. 3. The effective critical exponent $z\nu$ obtained from finite-size scaling analysis. The solid red lines show fitting curves based on the activated scaling law and gives $B_c^* = 20.0$ T in in-plane magnetic field (a) and $B_c^* = 18.8$ T in perpendicular magnetic field (b), respectively (see the vertical dashed red lines). The horizontal dashed magenta lines show $z\nu = 1$.

The infinite layer $Nd_{0.8}Sr_{0.2}NiO_2$ superconducting thin film shows the isotropic H_{c2} at low temperatures, as shown in Figs. S5 and S6 [55], consistent with previous studies [51–53]. The coherence length $\xi_{ab}(0) = 50.9 \pm 0.2$ Å and the superconducting thickness $d = 180 \pm 6$ Å, are extracted from data around T_c based on the Ginzburg-Landau theory [55]. Here, the deduced superconducting thickness d is about 2.4 times of the physical thickness ($d_{\text{exp}} \sim 7.6$ nm) of the film. Previously, the QGS are observed in conventional superconducting thin films with quenched disorder [42,44,45,49,50,77,80,81]. The in plane and perpendicular B_c^* of the QGS in conventional two-dimensional superconductors are anisotropic [49,50]. However, in unconventional nickelate superconducting thin films, the observed isotropic QGS with nearly similar zero-temperature critical field B_c^* cannot be understood by mean-field analysis and vortex physics, but indicates an unconventional microscopic origin.

To uncover the mechanism of isotropic QGS, we investigate the behavior of the metal state under high magnetic field ($> B_c^*$). For temperatures below 10 K down to 3 K, the sheet resistance shows the $\ln T$ dependence, as shown in Figs. 4(a) and 4(b). Moreover, for temperatures below ~1.5 K, the high-field resistance clearly follows a T^2 temperature dependence [insets of Figs. 4(a) and 4(b)], a clear feature of Kondo scattering [82,83]. These Kondo scattering features in $Nd_{0.8}Sr_{0.2}NiO_2$ samples are similar to previous results in underdoped $Nd_{1-x}Sr_xNiO_2$ samples [30], and help to illuminate the microscopic mechanism of the superconducting mechanism based on the extended t-J model with local Kondo interaction (t-J-K model) [4]. The schematic's physical pictures are shown in Figs. 4(c) and 4(d). The Kondo scattering between the mobile carrier of Nd/Sr and the local spin of Ni give rise to a Kondo singlet, which can also be considered as doublon. The doping effect results in a holon on a certain Ni site. Without a magnetic field, the superconducting fluctuation between these bosons (doublon and holon) can lead to boson condensation, and dramatically change the $R_s(T)$

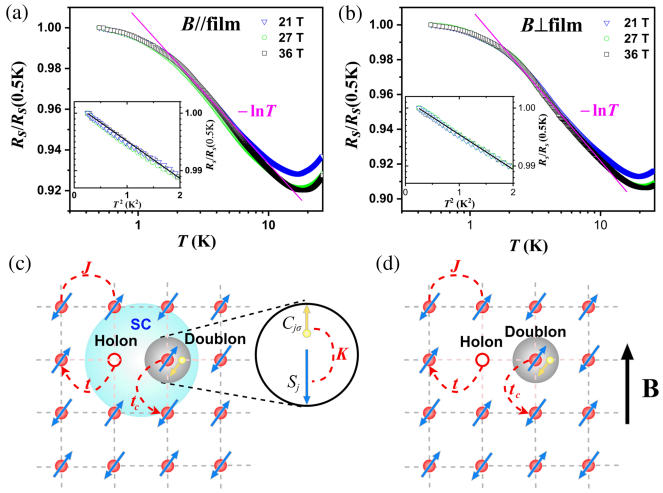

FIG. 4. The high-field temperature dependence of normalized sheet resistance of $Nd_{0.8}Sr_{0.2}NiO_2$ film under in-plane (a) and perpendicular (b) magnetic field, respectively. The blue triangles, green circles, and black squares represent renormalized sheet resistance $R_s(T)/R_s(0.5\ \mathrm{K})$ under magnetic field 21, 27, and 36 T, respectively. The pink lines represent the $\ln T$ dependence of R_s for temperatures below 10 K to 3 K. Insets in (a) and (b) show the T^2 behavior of R_s in the lowest temperature regime. (c),(d) The illustrations of the ***t*-*J*-*K*** model [4] on a two-dimensional square lattice of NiO_2 plane in $Nd_{0.8}Sr_{0.2}NiO_2$ under zero and high magnetic field B, respectively. The red balls with blue arrows represent the local spin 1/2 on the Ni site, interacting with its adjacent Ni spins through Heisenberg super-exchange coupling **J**. The yellow ball with an arrow denotes the electron of Nd, which couples to a Ni spin by the Kondo coupling **K**, to form a Kondo singlet (doublon). Red open circle represents Ni $3d^8$ configuration (holon). The **t** and $\mathbf{t_c}$ represent the hopping of holon and doublon, respectively. The light blue area in (c) represents the superconducting pairing between doublon and holon, which is broken down under high magnetic field, and the gray black cluster in (c) and (d) represents the Kondo cloud.

behavior from the Kondo scattering into a superconductor [55]. As a result, the local spin of Ni cannot give rise to resonance of the Yu-Shiba-Rusinov state, which is consistent with recent reports of STM experimental phenomena [34,84]. As the magnetic field strength increases, the superconducting coherence is destroyed, and the Kondo scattering characteristics reemerge. Meanwhile, around the phase boundary of SMT, the inhomogeneous distribution of the Kondo singlet gives rise to a superconducting island, and quantum percolation between these islands results in large rare regions. Thus, the formation of rare regions in $Nd_{0.8}Sr_{0.2}NiO_2$ superconducting thin film is irrelevant to the direction of an applied magnetic field, which is distinctive from those cases in conventional two-dimensional superconductors [42,44,45,49,50,77,80,81]. The observation of isotropic QGS in a nickelate superconductor may generate further research interest on the interplay between local magnetic moment and superconducting fluctuation in unconventional superconductors.

In conclusion, we systematically investigate the SMT driven by magnetic field in the unconventional $Nd_{0.8}Sr_{0.2}NiO_2$ superconductor. The finite-size scaling analysis shows strong evidence for the emergence of isotropic QGS under both in-plane and perpendicular magnetic fields. Moreover, the QGS-type activated scaling analysis can quantitatively explain the upturn of H_{c2} around zero temperature. The observed isotropic QGS in $Nd_{0.8}Sr_{0.2}NiO_2$ superconductor not only demonstrates the exotic quantum characteristics due to the superconducting fluctuation and Kondo scattering but can further arouse interest on quantum criticality in nickelate superconductors and other strong correlated superconducting systems.

This work was supported by the National Natural Science Foundation of China (92065110, 11974048, 12074334, and 12374037), and the Fundamental Research Funds for the Central Universities. The authors thank Prof. Ming-Liang Tian, from High Magnetic Field Laboratory of Chinese Academy of Sciences at Hefei, for his support with the high magnetic field measurements.

*These authors contributed equally to this letter.
†Contact author: haiwen.liu@bnu.edu.cn
‡Contact author: jcnie@bnu.edu.cn

[1] D. F. Li, K. Lee, B. Y. Wang, M. Osada, S. Crossley, H. R. Lee, Y. Cui, Y. Hikita, and H. Y. Hwang, Nature (London) **572**, 624 (2019).
[2] Y. Nomura and R. Arita, Rep. Prog. Phys. **85**, 052501 (2022).
[3] Q. Q. Gu and H. H. Wen, Innovation **3**, 100202 (2022).
[4] Y. F. Yang and G. M. Zhang, Front. Phys. **9**, 801236 (2022).
[5] C. Chen, R. Y. Ma, X. L. Sui, Y. Liang, B. Huang, and T. X. Ma, Phys. Rev. B **106**, 195112 (2022).
[6] M. Rossi *et al.*., Nat. Phys. **18**, 869 (2022).
[7] H. Lu, M. Rossi, A. Nag, M. Osada, D. F. Li, K. Lee, B. Y. Wang, M. Garcia-Fernandez, S. Agrestini, Z. X. Shen, E. M. Been, B. Moritz, T. P. Devereaux, J. Zaanen, H. Y. Hwang, K. J. Zhou, and W. S. Lee, Science **373**, abd7726 (2021).
[8] W. Z. Wei, D. Vu, Z. Zhang, F. J. Walker, and C. H. Ahn, Sci. Adv. **9**, eadh3327 (2023).
[9] X. R. Zhou, X. W. Zhang, J. B. Yi, P. X. Qin, Z. X. Feng, P. H. Jiang, Z. C. Zhong, H. Yan, X. N. Wang, H. Y. Chen, H. J. Wu, X. Zhang, Z. A. Meng, X. J. Yu, M. B. H. Breese, J. F. Cao, J. M. Wang, C. B. Jiang, and Z. Q. Liu, Adv. Mater. **34**, 2106117 (2022).
[10] N. N. Wang, M. W. Yang, Z. Yang, K. Y. Chen, H. Zhang, Q. H. Zhang, Z. H. Zhu, Y. Uwatoko, L. Gu, X. L. Dong, J. P. Sun, K. J. Jin, and J. G. Cheng, Nat. Commun. **13**, 4367 (2022).
[11] H. Ji, Y. Liu, Y. Li, X. Ding, Z. Xie, C. Ji, S. Qi, X. Gao, M. Xu, P. Gao, L. Qiao, Y.-F. Yang, G.-M. Zhang, and J. Wang, Nat. Commun. **14**, 7155 (2023).
[12] M. H. Xu, Y. Zhao, X. Ding, H. Q. Leng, S. Zhang, J. Gong, H. Y. Xiao, X. T. Zu, H. Q. Luo, K. J. Zhou, B. Huang, and L. Qiao, Front. Phys. **19**, 33209 (2024).

[13] X. Ding, Y. Fan, X. X. Wang, C. H. Li, Z. T. An, J. H. Ye, S. L. Tang, M. Y. N. Lei, X. T. Sun, N. Guo, Z. H. Chen, S. Sangphet, Y. L. Wang, H. C. Xu, R. Peng, and D. L. Feng, Natl. Sci. Rev. nwae194 (2024).
[14] Z. Yang, K. J. Jin, Y. L. Gan, C. Ma, Z. C. Zhong, Y. Yuan, C. Ge, E. J. Guo, C. Wang, X. L. Xu, M. He, D. X. Zhang, and G. Z. Yang, Small **19**, 2304146 (2023).
[15] W. Sun, Z. Jiang, C. Xia, B. Hao, Y. Li, S. Yan, M. Wang, H. Liu, J. Ding, J. Liu, Z. Liu, J. Liu, H. Chen, D. Shen, and Y. Nie, arXiv:2403.07344.
[16] S. Yan, W. Mao, W. Sun, Y. Li, H. Sun, J. Yang, B. Hao, W. Guo, L. Nian, Z. Gu, P. Wang, and Y. Nie, Adv. Mater. e2402916 (2024).
[17] W. Sun, Z. Wang, B. Hao, S. Yan, H. Sun, Z. Gu, Y. Deng, and Y. Nie, Adv. Mater. e2401342 (2024).
[18] M. C. Jung, H. LaBollita, V. Pardo, and A. S. Botana, Sci. Rep. **12**, 17864 (2022).
[19] J. Karp, A. Hampel, and A. J. Millis, Phys. Rev. B **105**, 205131 (2022).
[20] Z. Liu, Z. Ren, W. Zhu, Z. F. Wang, and J. L. Yang, npj Quantum Mater. **5**, 31 (2020).
[21] G. M. Zhang, Y. F. Yang, and F. C. Zhang, Phys. Rev. B **101**, 020501(R) (2020).
[22] R. Q. Zhang, C. Lane, B. Singh, J. Nokelainen, B. Barbiellini, R. S. Markiewicz, A. Bansil, and J. W. Sun, Commun. Phys. **4**, 118 (2021).
[23] M. A. Hayward and M. J. Rosseinsky, Solid State Sci. **5**, 839 (2003).
[24] A. Ikeda, Y. Krockenberger, H. Irie, M. Naito, and H. Yamamoto, Appl. Phys. Express **9**, 061101 (2016).
[25] Y. Fu, L. Wang, H. Cheng, S. Pei, X. Zhou, J. Chen, S. Wang, R. Zhao, W. Jiang, C. Liu, M. Huang, X. Wang, Y. Zhao, D. Yu, F. Ye, S. Wang, and J.-W. J. Mei, arXiv: 1911.03177.
[26] M. Franz, C. Kallin, A. J. Berlinsky, and M. I. Salkola, Phys. Rev. B **56**, 7882 (1997).
[27] J. Fowlie, M. Hadjimichael, M. M. Martins, D. F. Li, M. Osada, B. Y. Wang, K. Lee, Y. Lee, Z. Salman, T. Prokscha, J. M. Triscone, H. Y. Hwang, and A. Suter, Nat. Phys. **18**, 1043 (2022).
[28] G. Krieger, L. Martinelli, S. Zeng, L. E. Chow, K. Kummer, R. Arpaia, M. Moretti Sala, N. B. Brookes, A. Ariando, N. Viart, M. Salluzzo, G. Ghiringhelli, and D. Preziosi, Phys. Rev. Lett. **129**, 027002 (2022).
[29] Y. H. Guo, D. Qiu, M. X. Shao, J. Y. Song, Y. Wang, M. Y. Xu, C. Yang, P. Li, H. W. Liu, and J. Xiong, Adv. Mater. **35**, 33 (2023).
[30] T. N. Shao, Z. T. Zhang, Y. J. Qiao, Q. Zhao, H. W. Liu, X. X. Chen, W. M. Jiang, C. L. Yao, X. Y. Chen, M. H. Chen, R. F. Dou, C. M. Xiong, G. M. Zhang, Y. F. Yang, and J. C. Nie, Natl. Sci. Rev. **10**, nwad112 (2023).
[31] H. H. Chen, Y. F. Yang, G. M. Zhang, and H. Q. Liu, Nat. Commun. **14**, 5477 (2023).
[32] V. V. Poltavets, K. A. Lokshin, S. Dikmen, M. Croft, T. Egami, and M. Greenblatt, J. Am. Chem. Soc. **128**, 9050 (2006).
[33] S. Zeng, C. S. Tang, X. Yin, C. Li, M. Li, Z. Huang, J. Hu, W. Liu, G. J. Omar, H. Jani, Z. S. Lim, K. Han, D. Wan, P. Yang, S. J. Pennycook, A. T. S. Wee, and A. Ariando, Phys. Rev. Lett. **125**, 147003 (2020).
[34] Q. Q. Gu, Y. Y. Li, S. Y. Wan, H. Z. Li, W. Guo, H. Yang, Q. Li, X. Y. Zhu, X. Q. Pan, Y. F. Nie, and H. H. Wen, Nat. Commun. **11**, 6027 (2020).
[35] M. Osada, B. Y. Wang, B. H. Goodge, S. P. Harvey, K. H. Lee, D. F. Li, L. F. Kourkoutis, and H. Y. Hwang, Adv. Mater. **33**, 2104083 (2021).
[36] Q. Gao, Y. C. Zhao, X. J. Zhou, and Z. H. Zhu, Chin. Phys. Lett. **38**, 077401 (2021).
[37] D. F. Li, B. Y. Wang, K. Lee, S. P. Harvey, M. Osada, B. H. Goodge, L. F. Kourkoutis, and H. Y. Hwang, Phys. Rev. Lett. **125**, 027001 (2020).
[38] Q. K. Guo, S. Farokhipoor, C. Magen, F. Rivadulla, and B. Noheda, Nat. Commun. **11**, 9 (2020).
[39] Z. Q. Wang, Y. Liu, C. C. Ji, and J. Wang, Rep. Prog. Phys. **87**, 014502 (2024).
[40] S. C. Shen, Y. Xing, P. J. Wang, H. W. Liu, H. L. Fu, Y. W. Zhang, L. He, X. C. Xie, X. Lin, J. C. Nie, and J. Wang, Phys. Rev. B **94**, 144517 (2016).
[41] X. N. Wang, L. J. Wang, Y. X. Liu, F. Chen, W. P. Gao, Y. Wu, Z. L. Xu, W. Peng, Z. Wang, Z. F. Di, W. Li, G. Mu, and Z. R. Lin, Phys. Rev. B **107**, 094509 (2023).
[42] Y. Xing, H. M. Zhang, H. L. Fu, H. W. Liu, Y. Sun, J. P. Peng, F. Wang, X. Lin, X. C. Ma, Q. K. Xue, J. Wang, and X. C. Xie, Science **350**, 542 (2015).
[43] Y. C. Zhao, Y. Q. Su, Y. Q. Guo, J. Peng, J. Y. Zhao, C. Y. Wang, L. J. Wang, C. Z. Wu, and Y. Xie, ACS Mater. Lett. **3**, 210 (2021).
[44] Y. Xing, R. Zhao, P. J. Shan, F. P. Zheng, Y. W. Zhang, H. L. Fu, Y. Liu, M. L. Tian, C. Y. Xi, H. W. Liu, J. Feng, X. Lin, S. H. Ji, X. Chen, Q. K. Xue, and J. Wang, Nano Lett. **17**, 6802 (2017).
[45] Y. Saito, T. Nojima, and Y. Iwasa, Nat. Commun. **9**, 778 (2018).
[46] T. Vojta, Annu. Rev. Condens. Matter Phys. **10**, 233 (2019).
[47] H. J. Ji, H. W. Liu, H. Jiang, and X. C. Xie, Adv. Phys.-X **6**, 1884133 (2021).
[48] R. B. Griffiths, Phys. Rev. Lett. **23**, 17 (1969).
[49] C. Huang, E. Z. Zhang, Y. Zhang, J. L. Zhang, F. X. Xiu, H. W. Liu, X. Y. Xie, L. F. Ai, Y. K. Yang, M. H. Zhao, J. J. Qi, L. Li, S. S. Liu, Z. H. Li, R. Z. Zhan, Y. Q. Bie, X. F. Kou, S. Z. Deng, and X. C. Xie, Sci. Bull. **66**, 1830 (2021).
[50] Y. Liu, S. C. Qi, J. C. Fang, J. Sun, C. Liu, Y. Z. Liu, J. J. Qi, Y. Xing, H. W. Liu, X. Lin, L. L. Wang, Q. K. Xue, X. C. Xie, and J. Wang, Phys. Rev. Lett. **127**, 137001 (2021).
[51] B. Y. Wang, D. F. Li, B. H. Goodge, K. Lee, M. Osada, S. P. Harvey, L. F. Kourkoutis, M. R. Beasley, and H. Y. Hwang, Nat. Phys. **17**, 473 (2021).
[52] B. Y. Wang, T. C. Wang, Y. T. Hsu, M. Osada, K. Y. H. Lee, C. J. Jia, C. Duffy, D. F. Li, J. Fowlie, M. R. Beasley, T. P. Devereaux, I. R. Fisher, N. E. Hussey, and H. Y. Hwang, Sci. Adv. **9**, eadf6655 (2023).
[53] W. J. Sun, Y. Y. Li, R. X. Liu, J. F. Yang, J. Y. Li, W. Wei, G. J. Jin, S. J. Yan, H. Y. Sun, W. Guo, Z. B. Gu, Z. W. Zhu, Y. Sun, Z. X. Shi, Y. Deng, X. F. Wang, and Y. F. Nie, Adv. Mater. **35**, 7 (2023).
[54] W. Wei, W. J. Sun, Y. Sun, Y. Q. Pan, G. J. Jin, F. Yang, Y. Y. Li, Z. W. Zhu, Y. F. Nie, and Z. X. Shi, Phys. Rev. B **107**, L220503 (2023).

[55] See Supplemental Material at http://link.aps.org/supplemental/10.1103/PhysRevLett.133.036003, which includes Refs. [56–63], for additional information about the experimental characteristics and detailed discussions of the QGS and the t-J-K model, as well as the scaling analysis.
[56] H. Castro, J. Galvis, and S. Castro, IEEE Trans. Instrum. Meas. **60**, 198 (2011).
[57] K. Lee, B. H. Goodge, D. F. Li, M. Osada, B. Y. Wang, Y. Cui, L. F. Kourkoutis, and H. Y. Hwang, APL Mater. **8**, 041107 (2020).
[58] J. M. Kosterlitz and D. J. Thouless, J. Phys. C **6**, 1181 (1973).
[59] Y. L. Han, S. C. Shen, J. You, H. O. Li, Z. Z. Luo, C. J. Li, G. L. Qu, C. M. Xiong, R. F. Dou, L. He, D. Naugle, G. P. Guo, and J. C. Nie, Appl. Phys. Lett. **105**, 192603 (2014).
[60] W. H. Zhang *et al.*, Chin. Phys. Lett. **31**, 017401 (2014).
[61] L. E. Chow, K. Rubi, K. Y. Yip, M. Pierre, M. Leroux, X. Liu, Z. Luo, S. Zeng, C. Li, M. Goiran, N. Harrison, W. Escoffier, S. K. Goh, and A. J. Ariando, arXiv:2301.07606.
[62] D. S. Fisher, Phys. Rev. Lett. **69**, 534 (1992).
[63] T. Vojta, C. Kotabage, and J. A. Hoyos, Phys. Rev. B **79**, 024401 (2009).
[64] J. A. Hoyos, C. Kotabage, and T. Vojta, Phys. Rev. Lett. **99**, 230601 (2007).
[65] A. Del Maestro, B. Rosenow, J. A. Hoyos, and T. Vojta, Phys. Rev. Lett. **105**, 145702 (2010).
[66] S. Sachdev, P. Werner, and M. Troyer, Phys. Rev. Lett. **92**, 237003 (2004).
[67] A. Del Maestro, B. Rosenow, M. Müller, and S. Sachdev, Phys. Rev. Lett. **101**, 035701 (2008).
[68] L. S. Farrar, M. Bristow, A. A. Haghighirad, A. McCollam, S. J. Bending, and A. I. Coldea, npj Quantum Mater. **5**, 29 (2020).
[69] Z. T. Zhang, W. M. Jiang, T. N. Shao, Y. J. Qiao, X. Y. Chen, Q. Zhao, M. H. Chen, R. F. Dou, C. M. Xiong, and J. C. Nie, New J. Phys. **25**, 023023 (2023).
[70] Aslamazo. Lg and A. I. Larkin, Phys. Lett. **26A**, 238 (1968).
[71] Y. Liu, Y. Xu, J. Sun, C. Liu, Y. Z. Liu, C. Wang, Z. T. Zhang, K. Y. Gu, Y. Tang, C. Ding, H. W. Liu, H. Yao, X. Lin, L. L. Wang, Q. K. Xue, and J. Wang, Nano Lett. **20**, 5728 (2020).
[72] J. Shiogai, S. Kimura, S. Awaji, T. Nojima, and A. Tsukazaki, Phys. Rev. B **97**, 174520 (2018).
[73] Z. Chen, Y. Liu, H. Zhang, Z. R. Liu, H. Tian, Y. Q. Sun, M. Zhang, Y. Zhou, J. R. Sun, and Y. W. Xie, Science **372**, 721 (2021).
[74] C. Zhang, Y. J. Fan, Q. L. Chen, T. Y. Wang, X. Liu, Q. Li, Y. W. Yin, and X. G. Li, NPG Asia Mater. **11**, 76 (2019).
[75] E. Helfand and N. R. Werthamer, Phys. Rev. **147**, 288 (1966).
[76] R. A. Klemm, A. Luther, and M. R. Beasley, Phys. Rev. B **12**, 877 (1975).
[77] N. A. Lewellyn, I. M. Percher, J. J. Nelson, J. Garcia-Barriocanal, I. Volotsenko, A. Frydman, T. Vojta, and A. M. Goldman, Phys. Rev. B **99**, 054515 (2019).
[78] B. L. Brandt, D. W. Liu, and L. G. Rubin, Rev. Sci. Instrum. **70**, 104 (1999).
[79] D. S. Fisher, Phys. Rev. B **51**, 6411 (1995).
[80] Y. Saito, T. Nojima, and Y. Iwasa, Nat. Rev. Mater. **2**, 16094 (2017).
[81] Z. H. Cui, L. X. Pan, J. C. Fang, S. C. Qi, Y. Xing, H. W. Liu, Y. Liu, and J. Wang, J. Phys. D **56**, 374002 (2023).
[82] W. M. Star, C. Vanbaarl, E. Devroede, F. B. Basters, and G. M. Nap, Physica (Amsterdam) **58**, 585 (1972).
[83] Y. Matsushita, H. Bluhm, T. H. Geballe, and I. R. Fisher, Phys. Rev. Lett. **94**, 157002 (2005).
[84] R. F. Wang, Y. L. Xiong, H. Yan, X. P. Hu, M. Osada, D. F. Li, H. Y. Hwang, C. L. Song, X. C. Ma, and Q. K. Xue, Phys. Rev. B **107**, 115411 (2023).